An angular-spectrum approach to contrast in reflection acoustic microscopy

Abdullah Atalar

Edward L. Ginzton Laboratory, Stanford University, Stanford, California 94305
(Received 19 December 1977; accepted for publication 1 May 1978)

The scanning acoustic microscope in the reflection mode has proved to be a rather simple and direct means for monitoring the elastic properties of a solid surface. When smooth surfaces of crystalline material are examined in a liquid with a highly convergent sound beam they exhibit a distinct response. This characteristic response, which can be treated as a "signature", is obtained by recording the output of the microscope as the spacing between the acoustic lens and the object is varied. An angular-spectrum approach is used to derive an expression for this output in terms of the reflectance function. This function has an angular dependence determined by the bulk constants of the material itself. The expression resulting from this treatment can be used to explain the source of contrast in acoustic images.

PACS numbers: 43.20.Fn, 43.20.Bi, 68.25.+j, 62.20.Dc

I. INTRODUCTION

The scanning acoustic microscope[1-3] has been used to study the contour, texture, and structures of surfaces with a resolving power that continues to improve.[4] The changing contrast that appears in these micrographs has been described in a previous report[5] where we argued that the acoustic images give us detailed information on the surface elastic parameters for a scale of lateral dimensions that is determined by the diameter of the acoustic beam. It is our purpose in this paper to extend that original report and develop explicit expressions that will allow us to gain insight into the contrast variation that we have observed experimentally. This is accomplished here by using the angular-spectrum approach along with the paraxial approximation to calculate the variations in the signal that occur in reflection imaging when the object is moved through the focal plane. More general properties for these beams and their relation to image quality have been worked out by Wickramasinghe.[6] He computes the propagation parameters through angular-spectrum decomposition and calculates the beam profile for the case where the waves are strongly focused.

Our goal is the use of reflection imaging in the study of microscopic structures of increasing complexity, but we will first study the reflection from polished surfaces without structure. We have found that smooth surfaces of crystalline material exhibit a characteristic response that can be used to distinguish between different materials, to characterize the elastic properties of a given material, and to display variations in these properties on a microscopic scale that is limited only by the resolving power of the instrument.

In this instrument, the surface is immersed in liquid, and the liquid-solid interface is illuminated with a highly converging acoustic beam. The large difference in velocity between the liquid and the solid produces a critical angle for total internal reflection that is small compared to the critical angles that are usual in optical problems. Because of this factor, most of the illuminating beam is incident to the interface with angles which exceed the critical angle. We have found in this situation that the beam reflectance at the interface is a strong function of the nature of the surface being studied. We will show that the reflectance of single crystals of Si, Al_2O_3, and GaAs are quite different. These materials can be easily distinguished from each other if we observe the strength of the reflected signal while the distance between the acoustic lens and the reflector is varied.

We will follow the established procedure for problems of this type[7,8] and use Fourier transformations to decompose the entire beam into an angular spectrum of plane waves. In our model, the angular spectrum is symmetrically distributed about the normal to the interface since this direction corresponds to the axis of the beam in the actual experiment. In previous work relating to beams that undergo total internal reflection,[9-11] the beam is assumed to be obliquely incident to the interface. That work contains a clear description of the phase relation between the reflected and incident waves when the incident angle exceeds the critical angle for total internal reflection. It, therefore, has direct bearing on our work since these phase shifts dominate the reflection process in our model. For well-collimated beams obliquely incident to the interface, the phase shifts encountered upon reflection result in a reflected beam whose position is translated laterally along the reflecting surface. The lateral shift for optical beams is known as the "Goos-Hänchen shift".[12] For acoustic beams, the shift is known as the "Schoch displacement,"[13] and it is most pronounced when the acoustic beam is incident at the critical angle for Rayleigh-surface-wave excitation.[9]

In our problem, where the incident beam is normally incident to the interface there can be no lateral displacement for the entire beam. However, the phase shift experienced by each component does alter the wave front of the reflected beam in a manner that is unique for each reflecting surface. Our instrument is sensitive to the shape of this reflected wave front, and we have, therefore, in principle, a method for monitoring the elastic properties of this surface, obtained from the reflected wave when the spacing between the acoustic lens and the liquid-solid interface is varied. The electrical output of the transducer plotted as a function of this spacing produces a curve which differs from material to material. The curve for a given material is dramatically altered when metallic or dielectric layers are deposited on this material.

 0021-8979/78/4910-5130$01.10 © 1978 American Institute of Physics

We have long known that the acoustic microscope could be used to image surface features—features similar to those found in optical micrographs—but, with the insight that we have gained here, we now know that we can record information on the nature of the subsurface layers. In time, this characteristic—unique to acoustic microscopy—could prove to be most valuable in the study of materials and microscopic structures.

II. ACOUSTIC REFLECTION MICROSCOPE

In this section, we will briefly describe the acoustic reflection microscope with the essential parts of this acoustic imaging system as shown in Fig. 1.

Element A is a piezoelectric transducer which generates the acoustic wave. It serves to convert the rf voltage across the piezoelectric film into a plane acoustic wave propagating normal to the surface. Element B is the acoustic lens which is merely a spherical cavity on the opposing side of the crystal. It serves to focus the plane wave into a narrow waist at the focal point. Element C is the reflecting object to be imaged. A liquid, such as water, fills the gap between the object and the lens in order to provide a path for sound propagation. The reflected sound wave returns through the lens to the transducer which is now acting to convert the acoustic signal into the electrical signal. It is important to note that the transducer is sensitive to the phase of the returning wave and that the rf voltage at the output is obtained by integrating the acoustic field over the area of the transducer. A microwave circulator separates the reflected and incident signals. Normally, the object is near the focus point, and it is mechanically scanned in a raster pattern normal to the axis of the beam. The amplitude of the returning signal is used to control the intensity of a synchronously scanned electron beam in a cathode-ray tube (CRT). In this way, the image is displayed on the CRT, and it is recorded by photographing the face.

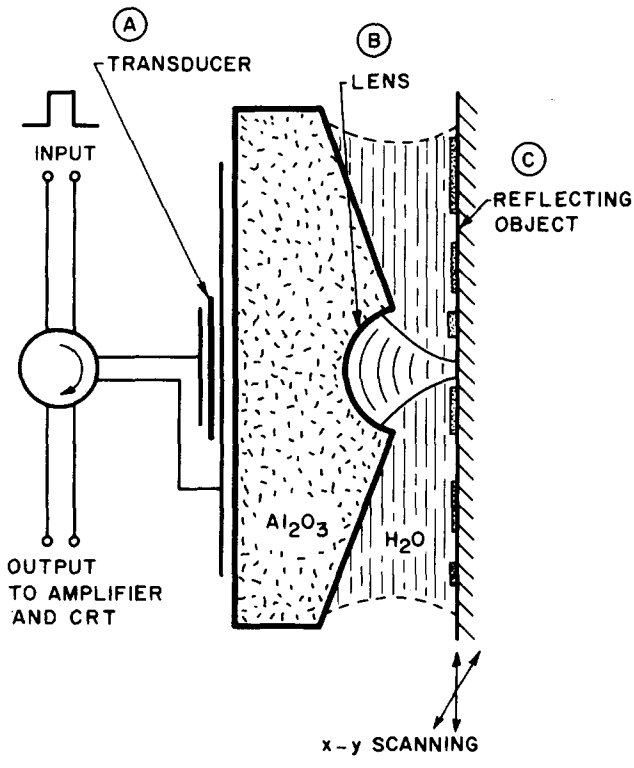

FIG. 1. Geometry of the acoustic transducer and lens as used for the acoustic microscope.

The acoustic lens has a radius R_l, and the focal distance f is given approximately by the relation

$$f=R_l/(1-\bar{c}) \quad \text{for } \bar{c}\ll 1.$$

Here, $\bar{c}$ is the ratio of the sound velocity in the liquid to that in the solid,

$$\bar{c}=v_{\text{liq}}/v_{\text{sol}}.$$

If $\bar{c}$ is small enough, the beam at the focus will be free from spherical aberration and the diameter of the waist will be limited only by diffraction. Therefore, the resolution of the system is determined by the wavelength in the liquid.

Finally, we note that a short pulse is used at the input, and time gating separates the reflected signal from other spurious reflections.

III. DESCRIPTION OF THEORY

The imaging system described in Sec. II will be analyzed using basic results reviewed in the Appendix. In Fig. 2, we show the coordinate system used for analysis. In the discussion that follows, the superscripts + and − refer to fields propagating in the $+z$ and $-z$ directions, respectively. Subscripts determine the z plane of the fields under consideration as defined below. We will assume monochromatic excitation throughout the discussion.

In Fig. 2, the planes labeled 1 and 2 represent the back and front focal planes of the lens, respectively. They are not

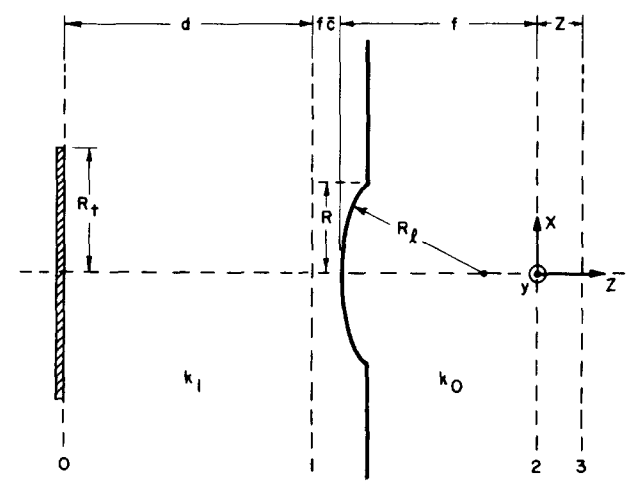

Fig. 2. Geometry and coordinate system used for analysis. Typical values: $R_t=105\,\mu$m, $R=75\,\mu$m, $R_l=104\,\mu$m, $f=120\,\mu$m, $\bar{c}=0.135$, $d=1230\,\mu$m.

at the same distance from the lens because of the different media involved. Plane 3 is the plane of the reflector, and it is a distance Z from the front focal plane (plane 2). R is the radius of the pupil function of the lens. If it is small enough compared to R_l, the thin-lens model can be used. As a result, the lens can be represented as a multiplicative phase transformation of the form

$$t_l = \exp[-j(k_0/2f)(x^2+y^2)],$$

where a constant phase factor is neglected. With the assumption of the thin-lens model, the following result can be established.[7]

Suppose an acoustical field represented by $u_1^+(x,y)$ is incident at the back focal plane of the lens (plane 1). The field $u_2^+(x,y)$ at the front focal plane (plane 2) can be found from the relation

$$u_2^+(x,y) = \frac{\exp[jk_0 f(1+\bar{c}^2)]}{j\lambda_0 f} \times \int_{-\infty}^{\infty}\int u_1^+(x_1,y_1)P_1(x_1+x_2,y_1+y_2) \times \exp\left[\left(-j\frac{2\pi}{\lambda_0 f}(x_1x_2+y_1y_2)\right)\right] dx_1\, dy_1. \tag{1}$$

Here, $P_1(x,y)$ stands for the pupil function of the lens, and it is given by

$$P_1(x,y) = \mathrm{circ}[(x^2+y^2)^{1/2}/R],$$

where

$$\mathrm{circ}(r) = 1, \quad r \leqslant 1,$$
$$= 0, \quad r > 1$$

for a circular lens with no apodization. Since we have a focused beam in the front focal plane, we are interested only in small values of x_2 and y_2, i.e., $x_2 \ll x_1$, $y_2 \ll y_1$. Hence,

$$P_1(x_1+x_2,y_1+y_2) \approx P_1(x_1,y_1).$$

With this assumption, the well-known Fourier transformation property of a lens can be stated as

$$u_2^+(x,y) = \frac{\exp[jk_0 f(1+\bar{c}^2)]}{j\lambda_0 f}\mathscr{F}[u_1^+(x,y)P_1(x,y)]\Big|_{\substack{k_x=k_0x/f\\ k_y=k_0y/f}}. \tag{2}$$

Propagation of this wave beyond the focal plane is easily calculated if the angular-spectrum representation is utilized. From Eq. (A1), we have

$$U_2^+(k_x,k_y) = \mathscr{F}[u_2^+(x,y)],$$

and combining this with Eq. (2), we arrive at the result

$$U_2^+(k_x,k_y) = \mathscr{F}\left(\frac{\exp[jk_0 f(1+\bar{c}^2)]}{j\lambda_0 f} \times \mathscr{F}[u_1^+(x,y)P_1(x,y)]\Big|_{\substack{k_x=k_0x/f\\ k_y=k_0y/f}}\right)$$

or

$$U_2^+(k_x,k_y) = -j\lambda_0 f \exp[jk_0 f(1+\bar{c}^2)] \times u_1^+[-(f/k_0)\,k_x, -(f/k_0)\,k_y] \times P_1[-(f/k_0)\,k_x, -(f/k_0)\,k_y]. \tag{3}$$

In Eq. (3), we relate the field on the back focal plane to the angular spectrum on the front focal plane with a simple relation.

After traversing the region of the lens, the acoustic field will propagate to plane 3 in Fig. 2 ($z=Z$ at this plane). This can be taken into account by using Eq. (A5) in the form

$$U_3^+(k_x,k_y) = U_2^+(k_x,k_y)\exp(jk_0Z) \times \exp\{-j[(k_x^2+k_y^2)/2k_0]Z\}. \tag{4}$$

Plane 3 is the interface between the liquid and the reflecting surface. At this plane, reflection takes place, and Eq. (A7) can be used to find the reflected field,

$$U_3^-(k_x,k_y) = U_3^+(k_x,k_y)\mathscr{R}(k_x/k_0, k_y/k_0), \tag{5}$$

where $\mathscr{R}$ is the reflectance function of the interface. The reflected field traveling in the $-z$ direction has an angular spectrum at $z=0$ given by the expression

$$U_2^-(k_x,k_y) = U_3^-(k_x,k_y)\exp(jk_0Z) \times \exp\{-j[(k_x^2+k_y^2)/2k_0]Z\}. \tag{6}$$

Here we have again made use of Eq. (A5). We can now combine Eqs. (3)–(6) to arrive at the result

$$U_2^-(k_x,k_y) = -j\lambda_0 f \exp[jk_0 f(1+\bar{c}^2)] \times u_1^+\left(-\frac{f}{k_0}k_x, -\frac{f}{k_0}k_y\right) \times P_1\left(-\frac{f}{k_0}k_x, -\frac{f}{k_0}k_y\right)$$

$$\times \exp(j2k_0 Z) \times \exp\left(-j\frac{k_x^2+k_y^2}{k_0}Z\right)$$

$$\times \mathscr{R}\left(\frac{k_x}{k_0}, \frac{k_y}{k_0}\right). \tag{7}$$

The acoustic field at this plane is found by inverse transforming $U_2^-(k_x,k_y)$,

$$u_2^-(x,y) = \mathscr{F}^{-1}[U_2^-(k_x,k_y)]. \tag{8}$$

The reflected field in the back focal plane (plane 1) is evaluated with an expression which corresponds to Eq. (1),

$$u_1^-(x_1,y_1) = \frac{\exp[jk_0 f(1+\bar{c}^2)]}{j\lambda_0 f}$$

$$\times \int_{-\infty}^{\infty}\int u_2^-(x_2,y_2) P_2(x_1+x_2, y_1+y_2)$$

$$\times \exp\left(-j\frac{2\pi}{\lambda_0 f}(x_1x_2+y_1y_2)\right) dx_2\, dy_2,$$

where $P_2(x,y)$ is the pupil function of the acoustic lens for waves traveling from the liquid side to the solid side. In the preceeding equation, $u_2^-(x_2,y_2)$ takes on significant values only when x_2 and y_2 are very small. Hence, we can again use the approximation $P_2(x_1+x_2, y_1+y_2) \approx P_2(x_1,y_1)$. With this assumption, we have

$$u_1^-(x,y) = \frac{\exp[jk_0 f(1+\bar{c}^2)]}{j\lambda_0 f} P_2(x,y)\ \mathscr{F}\{u_2^-(x,y)\}\Big|_{\substack{k_x=(k_0/f)x \\ k_y=(k_0/f)y}} \tag{9}$$

Equations (8) and (9) are combined to give

$$u_1^-(x,y) = \frac{\exp[jk_0 f(1+\bar{c}^2)]}{j\lambda_0 f} P_2(x,y)\ U_2^-\left(\frac{k_0}{f}x, \frac{k_0}{f}y\right). \tag{10}$$

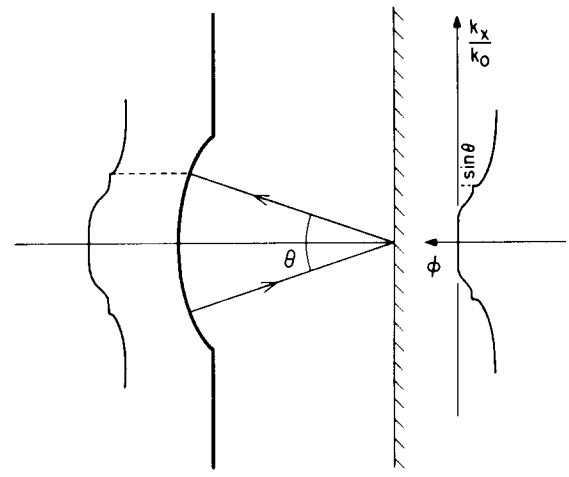

FIG. 3. Illustration of similarity between the phase of the reflected wave at the back focal plane and the phase of the reflectance function.

Equation (10) gives the field on one focal plane in terms of the angular spectrum on the other in a simple manner. Equations (3) and (10) are important results in the discussion, and they are rewritten in Table I, neglecting constant factors.

Finally, we can combine Eqs. (7) and (10) in the form

$$u_1^-(x,y) = -\exp\{j2k_0[Z+f(1+\bar{c}^2)]\}$$

$$\times u_1^+(-x,-y) P_1(-x,-y) P_2(x,y)$$

$$\times \exp[-j(k_0 Z/f^2)(x^2+y^2)]\mathscr{R}(x/f, y/f). \tag{11}$$

This is our primary result, and it expresses the reflected field at the back focal plane in terms of the incident field at the same plane, the pupil functions of the lens, the reflectance function of the reflector object, and the position of the object.

The factor $-\exp\{j2k_0[Z+f(1+\bar{c}^2)]\}$ is a constant phase factor, and from now on it will be neglected.

Some simple cases will be stated to give the reader some physical insight into the meaning of Eq. (11). Suppose there is a perfectly reflecting surface

TABLE I. Relations between the field and angular spectrum at the back and front focal planes.

Field at back focal plane (plane 1)	Propagation direction	Angular spectrum at front focal plane (plane 2)
$u_1^+(x,y)$	$\rightarrow$	$U_2^+(k_x,k_y) = u_1^+\left(-\frac{f}{k_0}k_x, -\frac{f}{k_0}k_y\right) P_1\left(-\frac{f}{k_0}k_x, -\frac{f}{k_0}k_y\right)$
$u_1^-(x,y) = P_2(x,y)\ U_2^-\left(\frac{k_0}{f}x, \frac{k_0}{f}y\right)$	$\leftarrow$	$U_2^-(k_x,k_y)$

$$\mathscr{R}(k_x/k_0,k_y/k_0)=1$$

at focal plane ($Z=0$). Then Eq. (11) becomes

$$u_1^-(x,y)=u_1^+(-x,-y)P_1(-x,-y)P_2(x,y).$$

$u_1^-(x,y)$ is equal to the inverted form of $u_1^+(x,y)$ after passing through the pupil functions. This is exactly what one would expect from the ray approach.

Suppose now that

$$\mathscr{R}(k_x/k_0,k_y/k_0)$$

has unit amplitude but nonzero phase. That is, let

$$\mathscr{R}(k_x/k_0,k_y/k_0)=\exp[j\phi(k_x/k_0,k_y/k_0)].$$

In this case, Eq. (11) gives

$$u_1^-(x,y)=u_1^+(-x,-y)P_1(-x,-y)P_2(x,y)$$

$$\times\exp[j\phi(x/f,y/f)].$$

This is demonstrated in Fig 3 for a two-dimensional case with an arbitrary function ϕ. $u_1^+(x)$ is assumed to be a plane wave, but $u_1^-(x)$ does not have a uniform phase because of the nonzero phase shift at the reflecting surface. The phase shift of $u_1^-(x)$ at x_0 is equal to the phase shift created upon reflection at the incidence angle $\theta=\sin^{-1}(x_0/f)$. Hence the reflected wave fronts at plane 1 take the shape of the function ϕ.

As another example, assume that the reflecting surface is not at the focal plane (i.e., $Z\neq 0$). For this situation, there is an additional phase curvature given by $\exp[-j(k_0/f^2)Z(x^2+y^2)]$.

After these simple examples, we can complete our analysis by transferring our input and output wave fronts to the transducer at the plane marked 0. We assume that the transducer excites a uniform field shown by $u_0^+(x,y)$, when a unit voltage is applied at its terminals, and that plane 0 is a distance d from plane 1. We want to find the transducer output voltage as a function of reflector parameters and Z, the distance between the reflector and front focal plane.

The field at plane 1 can be found from Eq. (A4),

$$u_1^+(x,y)=u_0^+(x,y)*\mathscr{F}^{-1}[\exp(jk_z'd)]. \tag{12}$$

similarly, the reflected field at plane 0 can be found in terms of $u_1^-(x,y)$,

$$u_0^-(x,y)=u_1^-(x,y)*\mathscr{F}^{-1}[\exp(jk_z'd)]. \tag{13}$$

In the receiving mode, the transducer will integrate the entire field to generate the output voltage. That means a plane wave with the wave fronts parallel to the film surface will yield a maximum electrical signal. The transducer output voltage, represented as a function of Z, is

$$V(Z)=\int_{-\infty}^{\infty}\int u_0^+(x',y')\,u_0^-(x',y')\,dx'\,dy'. \tag{14}$$

We can substitute Eq. (13) into Eq. (14) and write

$$V(Z)=\int_{-\infty}^{\infty}\int u_0^+(x',y')\left\{u_1^-(x',y')*\right.$$

$$\left.\times\mathscr{F}^{-1}[\exp(jk_z'd)]\Big|_{\substack{x=x'\\y=y'}}\right\}dx'dy'.$$

With the definition of convolution, this can be expressed as

$$V(Z)=\int_{-\infty}^{\infty}\int u_0^+(x',y')\left\{\int_{-\infty}^{\infty}\int u_1^-(\xi,\eta)\right.$$

$$\left.\times\mathscr{F}^{-1}[\exp(jk_z'd)]\Big|_{\substack{x=x'-\xi\\y=y'-\eta}}d\xi\,d\eta\right\}dx'\,dy'.$$

If we now change the order of integration, we find

$$V(Z)=\int_{-\infty}^{\infty}\int u_1^-(\xi,\eta)\left\{\int_{-\infty}^{\infty}\int u_0^+(x',y')\right.$$

$$\left.\times\mathscr{F}^{-1}[\exp(jk_z'd)]\Big|_{\substack{x=x'-\xi\\y=y'-\eta}}dx'\,dy'\right\}d\xi\,d\eta\,.$$

Since $k_z'=(k_1^2-k_x^2-k_y^2)^{1/2}$ is an even function of k_x and k_y, we can write

$$\mathscr{F}^{-1}[\exp(jk_z'd)]\Big|_{\substack{x=x'-\xi\\y=y'-\eta}}=\mathscr{F}^{-1}[\exp(jk_z'd)]\Big|_{\substack{x=\xi-x'\\y=\eta-y'}}.$$

With this in mind, we can recognize the integral inside the brackets as a convolution,

$$V(Z)=\int_{-\infty}^{\infty}\int u_1^-(\xi,\eta)$$

$$\times\left[u_0^+(\xi,\eta)*\mathscr{F}^{-1}[\exp(jk_z'd)]\Big|_{\substack{x=\xi\\y=\eta}}\right]d\xi\,d\eta.$$

This can be simplified with Eq. (12) to read

$$V(Z)=\int_{-\infty}^{\infty}\int u_1^-(\xi,\eta)\,u_1^+(\xi,\eta)\,d\xi\,d\eta\,, \tag{15}$$

and substituting Eq. (11) into Eq. (15), we have

$$V(z)=\int_{-\infty}^{\infty}\int u_1^+(-x,-y)\,u_1^+(x,y)$$

$$\times P_1(-x,-y)P_2(x,y)$$

$$\times\mathscr{R}(x/f,y/f)\exp[-j(k_0Z/f^2)(x^2+y^2)]\,dx\,dy. \tag{16}$$

Even though we have worked this out in rectangular coordinates, our problems are symmetric about the z axis, and we, therefore, prefer to write these results in cylindrical coordinates. With circular symmetry, we have

$$\mathscr{R}(k_x/k_0,k_y/k_0)=\mathscr{R}(k_r/k_0),$$

$$u_1^+(x,y)=u_1^+(r),$$

and

$$P(x,y)=P(r),$$

where $k_r=(k_x^2+k_y^2)^{1/2}$ and $r=(x^2+y^2)^{1/2}$. Therefore, the final result takes on the following form:

$$V(Z)=\int_0^\infty r\,[u_1^+(r)]^2P_1(r)P_2(r)\ \mathscr{R}(r/f)$$

$$\times\exp[-j(k_0Z/f^2)r^2]\,dr, \tag{17}$$

where a factor of 2π is neglected.

IV. APPLICATIONS

Using the final result in Sec. III, several cases that give answers in closed form can be worked through.

Case 1

Let $u_1^+(r)=1$, $\mathscr{R}(k_r/k_0)=1$, and $P_1(r)=P_2(r)=\mathrm{circ}(r/R)$ (perfect reflector). From Eq. (17), we can write immediately

$$V(Z)=\int_0^R r\exp\left(-j\frac{k_0}{f^2}Zr^2\right)dr$$

$$=\frac{R^2}{2}\exp\left(-j\frac{\pi R^2}{\lambda_0 f^2}Z\right)$$

$$\times\left(\frac{\sin(\pi R^2/\lambda_0 f^2)Z}{(\pi R^2/\lambda_0 f^2)Z}\right).$$

Equation (17) predicts that if a perfect reflector is translated along the z-axis the transducer output voltage will change in accordance with a sinc function. When the object is at focus ($Z=0$), the output voltage is maximum, since the returning wave fronts are parallel to the transducer film. However, for positive Z (object-lens spacing increasing) or negative Z (object-lens spacing decreasing), the transducer response is reduced. The reflected wave reaching the transducer is in the form of either a spherically converging or diverging wave, and the transducer is excited with alternate regions of positive and negative phase.

Case 2

Let

$$u_1^+(r)=1, P_1(r)=P_2(r)=\mathrm{circ}(r/R)$$

and

$$\mathscr{R}(k_r/k_0)=\exp[-j2\pi(fk_r/Rk_0)^2].$$

Here the reflectance function has a unit amplitude and a nonzero phase shift. For this case, Eq. (17) gives

$$V(Z)=\frac{R^2}{2}\exp\left[-j\frac{\pi R^2}{\lambda_0 f^2}\left(Z+\frac{\lambda_0 f^2}{R^2}\right)\right]$$

$$\times\frac{\sin(\pi R^2/\lambda_0 f^2)\ [Z+(\lambda_0 f^2/R^2)]}{(\pi R^2/\lambda_0 f^2)\ [Z+(\lambda_0 f^2/R^2)]}.$$

This is merely a sinc function shifted along the Z axis. The maximum output voltage is not reached when the object is at focus, but rather when it is at $Z=-(\lambda_0 f^2/R^2)$. The wavefront distortion produced by this form of a reflector is compensated by moving the reflector out of focus and thereby creating a plane wave front at the transducer.

Case 3

Let

$$u_1^+(r)=1,\ P_1(r)=P_2(r)=\mathrm{circ}(r/R)$$

and

$$\mathscr{R}(k_r/k_0)=0,\quad k_r/k_0<R_1/f,$$

$$=1,\quad k_r/k_0>R_1/f.$$

Here an object is assumed which reflects only when the incidence angle is greater than some critical angle [$\theta_c=\sin^{-1}(R_1/f)$ in this case]. Equation (17) gives

$$V(Z)=\frac{R^2-R_1^2}{2}\exp\left(-j\frac{\pi}{\lambda_0 f^2}(R^2+R_1^2)Z\right)$$

$$\times\frac{\sin(\pi/\lambda_0 f^2)(R^2-R_1^2)Z}{(\pi/\lambda_0 f^2)(R^2-R_1^2)Z}.$$

We still obtain a sinc function, but the width of the main lobe is increased as a result of the given reflectance function.

Note in the examples above that the transducer output voltage not only depends on the object position but also on the reflectance function. This gives rise to a mechanism to differentiate the objects with different acoustical properties because the reflectance function will depend on the elastic properties of the object.

To gain a deeper understanding, we will select examples from real life. Single crystals of silicon, saphire, and gallium arsenide will be taken as reflector objects, and the corresponding reflectance functions will be calculated. Equation (17) will be used to determine the output voltage in terms of reflector position for these crystals.

The amplitude and phase of the reflectance function will first be evaluated at a liquid-solid interface. Figure 4(a) is a plot of these two parameters for a water-silicon interface.[14] The variable $\sin\theta=(k_r/k_0)$ is used rather than the angle of incidence. Here k_r is the projection of wave vector k_0 onto the x-y plane. In these terms, the angle of incidence is given by $\theta=\sin^{-1}(k_r/k_0)$. The amplitude of the reflectance function is slightly less than unity when the incident angle is less than the "critical angle for shear waves". The first narrow peak corresponds to the "critical angle for longitudinal waves". The phase, on the other hand, is zero up to the longitudinal critical angle and has a transition at the Rayleigh critical angle (slightly greater than the shear critical angle).

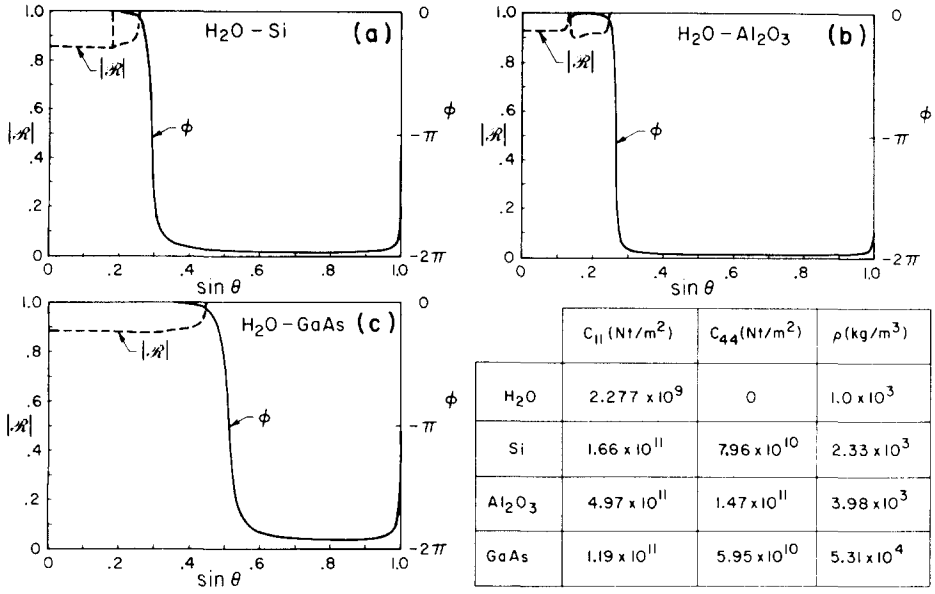

	C_{11} (Nt/m^2)	C_{44} (Nt/m^2)	ρ (kg/m^3)
H_2O	2.277×10^9	0	1.0×10^3
Si	1.66×10^{11}	7.96×10^{10}	2.33×10^3
Al_2O_3	4.97×10^{11}	1.47×10^{11}	3.98×10^3
GaAs	1.19×10^{11}	5.95×10^{10}	5.31×10^4

FIG. 4. Reflectance function for various interfaces as a function of $\sin\theta$, where θ is the angle of incidence for plane waves. The reflectance function is given by $|\mathscr{R}|\exp(j\phi)$ The table shows the acoustic parameters used in calculation.

For angles greater than this, the phase shift approaches -2π. The corresponding curves for Al_2O_3 and GaAs are shown in Figs. 4(a) and 4(c). These curves are calculated with an isotropic-solid assumption.

The solid curves in Figs. 5(b)–5(d) show the calculated output voltage magnitude versus object position for those materials. Calculations are based on Eq. (17). The incident field $u_1^+(r)$ is calculated once assuming an isotropic propagation medium,[15] and then Eq. (17) is used to give the output voltage for each of the different materials. $P_1(r)$ and $P_2(r)$ in Eq. (17) are the effective pupil functions of the acoustic lens for waves traveling from solid to liquid and from liquid to solid, respectively. If $u_2^-(r)$ was equal to $u_2^+(r)$, the problem would be perfectly symmetrical, and P_1 should be equal to P_2 from a reciprocity argument.[16] In general, this condition is not satisfied, but we will assume that P_1 and P_2 are approximately equal. They include the effect of the matching layer on the lens surface as well as the finite aperture of the lens.[16] Figure 5(a) shows the result of the calculations for the amplitude and the phase of $[u_1^+(r)]^2 P_1(r)P_2(r)$ which is used in the computation of $V(Z)$ curves. The nonzero phase of $[u_1^+(r)]^2 P_1(r)P_2(r)$ is the reason why $V(Z)$ curves do not have a maximum at $Z=0$. This phase curvature creates a focal shift of about $2\,\mu$m. In Figs. 5(b)–5(d), our experimental results are also indicated. The experimental and theoretical curves for Si and Al_2O_3 are in good agreement, supporting the validity of our approach. The discrepancy in fit for GaAs is attributed to the relatively high anisotropy of GaAs.

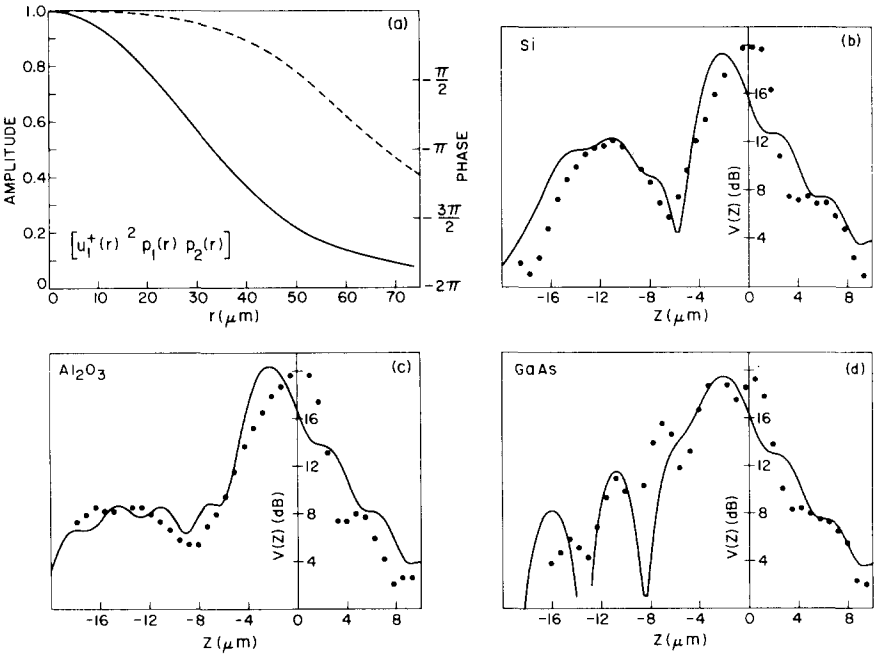

FIG. 5. (a) shows the magnitude (solid line) and the phase (dashed line) of $u_1^+(r)^2 P_1(r)P_2(r)$. (b)–(d) are the calculated output voltage magnitude versus object position for various crystals at $f=1100$ MHz. The dotted points are the measured response.

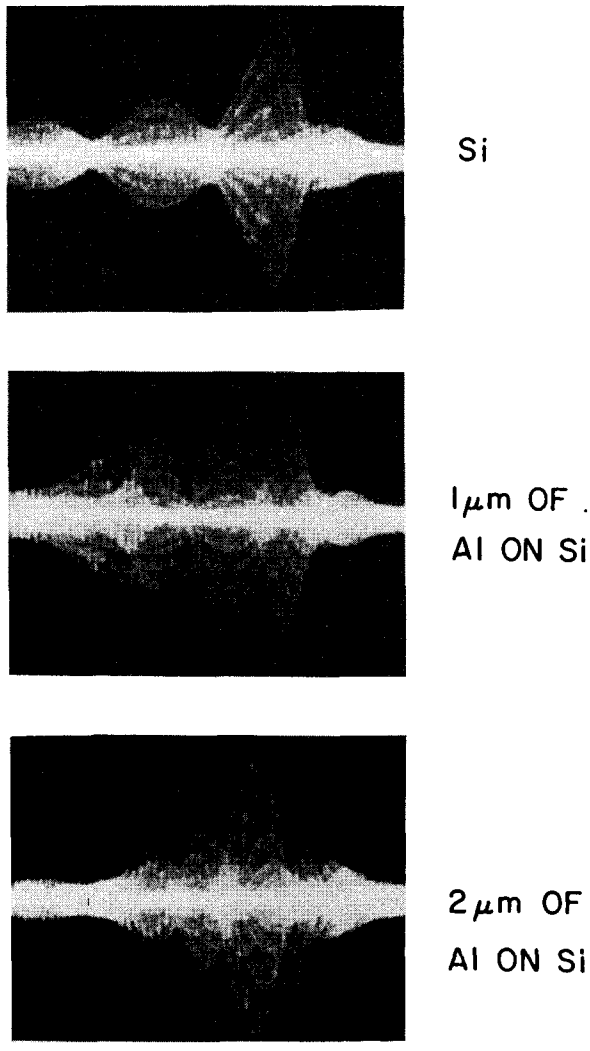

FIG. 6. Long-exposure oscilloscope photos of the returning pulses from the sample as they appear on the scope face while the sample is moving through the axis. Upper envelopes correspond to $V(Z)$ curves at $f = 1100$ MHz. Horizontal scale: 3.75 μm/div.

Recall that the reflectance functions are calculated assuming an isotropic solid (C_{12} is neglected).

The informational content of the $V(Z)$ curves can be further amplified by a presentation of the form shown in Fig. 6. These are long-exposure oscilloscope photos of the returning pulses from the sample as they appear on the scope face while the sample is moving through the axis. The triggering of the trace is such that the horizontal scale on the scope is a direct measure of the lens-to-sample spacing. It is only the upper envelope of these traces that is significant, and the structure beneath the envelope should be ignored. Figure 6 shows the $V(Z)$ photos for pure Si, 1.0 μm of Al on Si and 2.0 μm of Al on Si, with an acoustic excitation frequency of 1100 MHz.

The $V(Z)$ curves are unique to the materials' acoustic properties and, therefore, can be treated as a "signature" of the material. As an obvious application, this signature can be used to determine the thickness of a layer on a substrate by

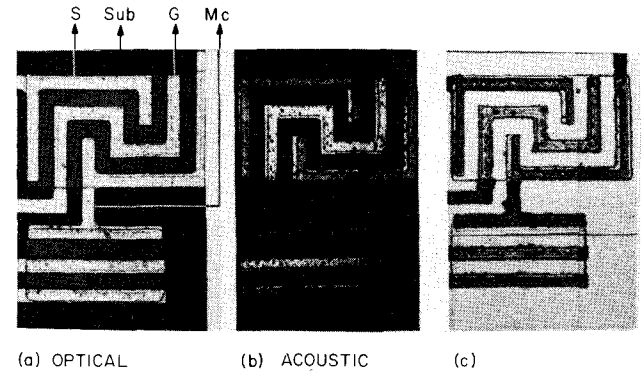

FIG. 7. Optical and acoustical pictures of two H-MOS transistors. Source (S): $Al_2O_3 + 0.9\,\mu m\ Si + 1.2\,\mu m\ Al + 0.4\,\mu m\ SiO_2$. Gate (G): $Al_2O_3 + 0.9\,\mu m\ Si + 0.1\,\mu m\ SiO_2 + 1.2\,\mu m\ Al + 0.4\,\mu m\ SiO_2$. Metal connection (MC): $Al_2O_3 + 1.2\,\mu m\ Al + 0.4\,\mu m\ SiO_2$. Substrate (Sub): $Al_2O_3 + 0.4\,\mu m\ SiO_2$.

comparing the resulting curve to the curves of similar samples with known layer thicknesses. It should be noted that the curves for layered media will depend on the frequency of acoustic excitation, so the comparison must be done at the same frequency.

A sample such as an integrated circuit contains various layers made up of different materials. If an acoustic image of that sample is recorded, the z position remains constant while the x-y scanning is carried out. Each particular region on the sample gives rise to a response determined by its own $V(Z)$ curve at that z position. This response may differ considerably from region to region (as much as 20 dB). That is a primary source of contrast for acoustic imaging.

In Fig. 7(a), we show an optical picture of two H-MOS transistors on an SOS chip.[17] The acoustic images in Figs. 7(b) and 7(c) were recorded at a frequency of 1100 MHz where the wavelength in water is about 1.4 μm. There we estimate the resolution to be near 1 μm. The only difference between Figs. 7(b) and 7(c) is the Z position of the object. An almost complete contrast reversal is obtained only by changing the axial position of the object. Note that the gate regions are brighter than the source or drain in both acoustical pictures, whereas they have the same brightness in the optical case. Acoustic images, therefore, include the response of layers beneath the surface. In this particular case, the presence of a 1000-Å oxide layer underneath a 1-μm-thick gate metal is responsible for the recorded difference.

In Fig. 8, we show the calculated $V(Z)$ curves for the various regions on the transistor geometry.[18] The position of the object with respect to the focal point (parameter Z) determines the relative brightness in various regions. The acoustic image shown in Fig. 7(b) is taken at a position indicated as (b) on Fig. 8. At this position, the output voltage is larger for the gate than it is for the source. The response for other regions is much lower, and this accounts for the dark background in the acoustic image. On the other hand, the acoustic micrograph shown in Fig. 7(c) is taken with the position shown as (c) in Fig. 8. The gate region should still be brighter than the source or drain, but the background gives rise to a much higher output voltage or brightness. It should

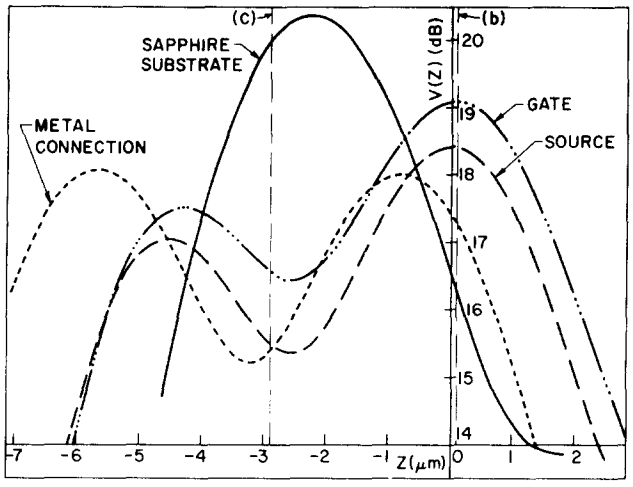

FIG. 8. Calculated $V(Z)$ curves for various regions on the SOS structure.

be noted that, if the oxide under the gate metal was missing, the gate in the acoustic picture would correspond in brightness to that of the source or drain rather than the brightness shown here.

V. CONCLUSIONS AND SUMMARY

Using an angular-spectrum approach, it was possible to arrive at a relatively simple expression which formulates the microscope response in terms of the position and elastic parameters of the reflector. This approach also made it possible to gain a physical insight into the underlying mechanism. From this work, we have learned that the reflectance function as transferred to the reflected wave front can be revealed to the outside world by translating the object through the focused beam and recording the transducer output voltage. This signature can be used to explain the source of high contrast in many acoustic images.

In principle, the theory given applies to optical waves as well. However, the physical realization of an analog optical scanning system is not obvious, since an optical detector which integrates field rather than intensity is needed. Furthermore, critical angles for optical waves are often much larger than those encountered here.

Reflection acoustic microscopy can find applications in monitoring layer thicknesses and nondestructive fault analysis of integrated circuits. One example of an acoustic image is given in this paper, and this displays information that is not found in the optical picture.

ACKNOWLEDGMENTS

The author wishes to express his appreciation to Professor C.F. Quate for his insight, guidance, and encouragement during the course of this work. He also wishes to thank H.K. Wickramasinghe for providing us with the acoustic reflection program for layered media prior to publication, Rockwell International for supplying the SOS sample, the late Professor R. Kompfner for valuable suggestions, and V. Jipson and S. Ayter for helpful discussions. This work was supported by the National Bureau of Standards (Contract No. 5-35899) and the Air Force Office of Scientific Research (Grant No. AFOSR-77-3455).

APPENDIX: ANGULAR-SPECTRUM REPRESENTATION

This appendix summarizes the primary results that are used to decompose a complicated wave front into an angular spectrum of plane waves by means of the Fourier transform.[7,8] This method is a powerful technique for treating wave propagation in a homogeneous isotropic half-space that is free from sources.

Now suppose that a monochromatic wave is incident at the $z=z_1$ plane and that it is traveling in the z direction. The complex field of this wave is given by $u_1(x,y)$ with $\exp(-j\omega t)$ time dependence suppressed. The angular spectrum in this plane is then given by the relation

$$U_1(k_x,k_y)=\mathscr{F}[u_1(x,y)] = \iint_{\infty}^{-\infty} u_1(x,y)\exp[-j(k_x x+k_y y)]\,dx\,dy. \tag{A1}$$

In this representation, we decompose the field $u_1(x,y)$ into plane wave components of the form $\exp\{j[k_x x+k_y y+k_z(z-z_1)]\}$ having an amplitude $U_1(k_x,k_y)$). Here $\exp[j(k_x x+k_y y)]$ represents a unit amplitude plane wave incident on the $z=z_1$ plane with an angle

$$\theta=\sin^{-1}[(k_x^2+k_y^2)^{1/2}/k_0],$$

where $k_0=(\omega/v_0)$.

The angular spectrum at another plane, $z=z_2$, can be found by multiplying $U_1(k_x,k_y)$ by $\exp[jk_z(z_2-z_1)]$, where $k_z=(k_0^2-k_x^2-k_y^2)^{1/2}$ to give

$$U_2(k_x,k_y)=U_1(k_x,k_y)\exp[jk_z(z_2-z_1)]. \tag{A2}$$

Note that for $k_x^2+k_y^2>k_0^2$, k_z is purely imaginary, and corresponding plane waves are evanescent.

With the spectrum in this form, the complex field at $z=z_2$ can be determined by inverse transforming

$$u_2(x,y)=\mathscr{F}^{-1}[U_2(k_x,k_y)] = [1/(2\pi)^2]\iint_{-\infty}^{\infty} U_2(k_x,k_y) \times\exp[j(k_x x+k_y y)]\,dk_x\,dk_y. \tag{A3}$$

In the space domain, Eq. (A2) can be written as

$$u_2(x,y)=u_1(x,y)*\mathscr{F}^{-1}\{\exp[jk_z(z_2-z_1)]\}, \tag{A4}$$

where * signifies the convolution operation. If the so-called paraxial approximation is used, the expressions can be simplified, since we have

$$(k_0^2-k_x^2-k_y^2)^{1/2}\approx k_0-\tfrac{1}{2}[(k_x^2+k_y^2)/k_0] \quad \text{for } (k_x^2+k_y^2)\ll k_0,$$

and with this we can write

$$\exp[jk_z(z_2-z_1)]\approx\exp[jk_0(z_2-z_1)]$$

$$\times \exp\left(-j\frac{k_x^2+k_y^2}{2k_0}(z_2-z_1)\right). \tag{A5}$$

The first exponential factor in Eq. (A5) is an overall phase retardation suffered by any component of the angular spectrum as it propagates from $z=z_1$ to $z=z_2$. The second factor, however, is a phase dispersion with a quadratic frequency dependence on the spatial angle.

With this approximation, Eq. (A2) can be written as

$$U_2(k_x,k_y) \approx U_1(k_x,k_y)\exp[jk_0(z_2-z_1)] \times \exp\left(-j\frac{k_x^2+k_y^2}{2k_0}(z_2-z_1)\right). \tag{A6}$$

Now let a second region be introduced separated from the first region by a plane boundary at $z=z_3$. If a plane wave of the form $U_3(k_x,k_y)\exp\{j[k_x x+k_y y+k_z(z-z_3)]\}$ is incident on this boundary, there will be a reflected plane wave of the form $U_3'(k_x,k_y)$ $\exp\{j[k_x x+k_y y-k_z(z-z_3)]\}$. Suppose that the reflectance function

$$\mathscr{R}(k_x/k_0,k_y/k_0)$$

of the boundary is known. This function relates $U_3'(k_x,k_y)$ to $U_3(k_x,k_y)$ as follows:[10]

$$U_3'(k_x,k_y)=\mathscr{R}(k_x/k_0,k_y/k_0)U_3(k_x,k_y). \tag{A7}$$

This reflectance function

$$\mathscr{R}(k_x/k_0,k_y/k_0)$$

is, in general, a complex function, and it therefore includes phase changes as well as amplitude changes upon reflection.

[1]R.A. Lemons and C.F. Quate, Appl. Phys. Lett. **25**, 251 (1974).
[2]C.F. Quate, Electrochemical Society Meeting, Philadelphia, 1977 (unpublished).
[3]R.G. Wilson, R.D. Weglein, and D.M. Bonnell (unpublished).
[4]V. Jipson and C.F. Quate, Appl. Phys. Lett. **32**, 789 (1978).
[5]A. Atalar, C.F. Quate, and H.K. Wickramasinghe, Appl. Phys. Lett. **31**, 791 (1977).
[6]H.K. Wickramasinghe, (unpublished).
[7]J.W. Goodman, *Introduction to Fourier Optics* (McGraw-Hill, New York, 1968), p. 48.
[8]D.C. Champeney, *Fourier Transforms and Their Physical Applications* (Academic, London, 1973), p. 142.
[9]M.A. Breazeale, L. Adler, and G.W. Scott, J. Appl. Phys. **48**, 530 (1977).
[10]M. McGuirk and C.K. Carniglia, J. Opt. Soc. Am. **67**, 103 (1977).
[11]P.K. Tien, Rev. Mod. Phys. **49**, 361 (1977).
[12]F. Goos and H. Hänchen, Ann. Phys. (Leipzig) **1**, 333 (1947).
[13]A. Schoch, Ergeb. Exacten Naturwiss. **23**, 127 (1950); Acustica **2**, 18 (1952).
[14]L.M. Brekhovskikh, *Waves in Layered Media* (Academic, New York, 1960).
[15]J. Zemanek, J. Acoust. Soc. Am. **49**, 181 (1971).
[16]R.A. Lemons, Ph.D. thesis (Standford University, 1975) (unpublished), available from University Microfilms, Ann Arbor, Mich. RPT. No. 75-25, 562.
[17]This picture was taken with a Zeiss bright-field reflection microscope as furnished to us by R. Koch.
[18]The computer program to calculate the reflection function $\mathscr{R}$ for layered media was furnished to us by H.K. Wickramasinghe.